VOL. 14, NO. 13, JULY 2019 ISSN 1819-6608
ARPN Journal of Engineering and Applied Sciences
©2006-2019 Asian Research Publishing Network (ARPN). All rights reserved.
www.arpnjournals.com

UNSTEADY MHD FLOW THROUGH POROUS MEDIUM IN A ROTATING VERTICAL CHANNEL IN SLIP FLOW REGIME

N. Ravi Kumar and R. Bhuvana Vijaya
Department of Mathematics, JNTUA College of Engineering, Ananthapuramu, Andhra Pradesh, India
E-Mail: ravinandyala@gmail.com

ABSTRACT

We consider an oscillatory MHD convective viscous incompressible, radiating and electrically conducting second grade fluid through porous medium in a vertical rotating channel in slip flow regime. A flow is laminar and fully developed and the fluid is presupposed to be gray, absorbing and emitting radiation out in non scattering medium. The solutions are obtained for the velocity and temperature distributions making use of regular perturbation technique. The velocity, temperature and concentration profiles are discussed through graphically as well as skin friction coefficient, Nusselt number and Sherwood number are evaluated numerically and presented in the form of tables.

Keywords: radiating fluid, MHD oscillatory flow, rotating channel, slip flow regime.

Nomenclature

(u, v)	the velocity components along x and y directions
p	the modified pressure
t	time
C_p	Specific heat
B_0	electromagnetic induction
g	Acceleration due to gravity
K_1	thermal conductivity
k	permeability of the porous medium
Q_0	Heat absorption
T	temperature of the fluid
f_1	Maxwell's reflection co-efficient
μ	Co-efficient of viscosity
L	mean free path
T_0	mean temperature
w_0	suction velocity
q_1	radiative heat
q	Complex velocity
M	Hartmann number
K	Permeability parameter
S	second grade fluid parameter
E	Ekman number
Gr	thermal Grashof number
Pr	Prandtl number
m	Hall parameter
D	the molecular diffusivity
K_c	the chemical reaction parameter
C	concentration
C_0	mean concentration
Q_1	Radiation absorption

Greek symbols

α	the mean variation absorption coefficient
α_1	normal stress moduli
θ	Dimension less temperature
ϕ	Dimension less concentration
Ω	Angular velocity
σ	Electrical conductivity of the fluid
ρ	Density of the fluid
ν	Kinematic viscosity
ω	the frequency of oscillation
β	The coefficient of volume expansion
β_c	The coefficient of volume expansion with concentration

1. INTRODUCTION

The wall slip flow is a very important phenomenon that is widely encountered in this era of industrialization. It has numerous applications, for example in lubrication of mechanical devices where a thin film of lubricant is attached to the surface slipping over one another or when the surfaces are coated with special coatings to minimize the friction between them. Marques *et al* [1] have considered the effect of the fluid slippage at the plate for Couette flow. Hayat *et al*. [2] analyzed slip flow and heat transfer of a second grade fluid past a stretching sheet through a porous space.

The magneto hydrodynamic (MHD) flow of a viscoelastic fluid as a lubricant is also of primary interest in many industrial applications. The MHD lubrication is an externally pressurized thrust that has been investigated both theoretically and experimentally by Maki *et al* [3]. Hughes and Elco [4] have investigated the effects of magnetic field in lubrication. Hamza [5] considered the squeezing flow between two discs in the presence of a magnetic field. The problem of squeezing flow between rotating discs has been studied by Hamza [6] and Bhattacharya and Pal [7]. Sweet *et al*. [8] solved analytically the problem of unsteady MHD flow of a viscous fluid between moving parallel plates. Hayat *et al*. [9] have presented analytical solution to the unsteady rotating MHD flow of an incompressible second grade fluid in a porous half space. There is a variety of industrial applications wherein due to high temperature radiative

©2006-2019 Asian Research Publishing Network (ARPN). All rights reserved.

heat is also accompanied along with conduction and convection heat. Algoa *et al.* [10] studied the radiative and free convective effects on a MHD flow through a porous medium between infinite parallel plates with time-dependent suction. Mebine and Gumus [11] investigated steady-state solutions to MHD thermally radiating and reacting thermosolutal flow through a channel with porous medium.

Recently, Krishna and Swarnalathamma [12] discussed the peristaltic MHD flow of an incompressible and electrically conducting Williamson fluid in a symmetric planar channel with heat and mass transfer under the effect of inclined magnetic field. Swarnalathamma and Krishna [13] discussed the theoretical and computational study of peristaltic hemodynamic flow of couple stress fluids through a porous medium under the influence of magnetic field with wall slip condition. Veera Krishna and Gangadhar Reddy [14] discussed MHD free convective rotating flow of visco-elastic fluid past an infinite vertical oscillating plate. Veera Krishna and Subba Reddy [15] discussed unsteady MHD convective flow of second grade fluid through a porous medium in a Rotating parallel plate channel with temperature dependent source.

In view of the above facts, in this chapter, we have considered an oscillatory MHD convective viscous incompressible, radiating and electrically conducting second grade fluid through porous medium in a vertical rotating channel in slip flow regime.

2. FORMULATION AND SOLUTION OF THE PROBLEM

We consider an oscillatory MHD convective viscous incompressible, radiating and electrically conducting second grade fluid through porous medium in a vertical rotating channel in slip flow regime. A flow is bounded by two infinite vertical insulated plates at *d* distance apart with uniform transverse magnetic field B_0 normal to the channel.

We introduce a Cartesian co-ordinate system with *x*-axis oriented vertically upward along the centreline of this channel and *z*-axis taken perpendicular to the planes of the plates which is the axis of the rotation and the entire system comprising of the channel and the fluid are rotating as a solid body about this axis with constant angular velocity Ω. A constant injection velocity w_0 is applied at the plate $z=-d/2$ and the same constant suction velocity, w_0, is applied at the plate $z=d/2$. The schematic diagram of the physical problem is shown in the Figure-1.

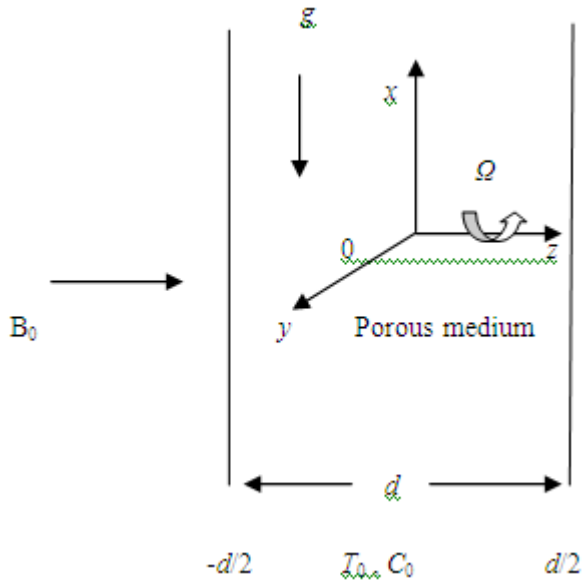

Figure-1. Schematic diagram.

Since the plates of the channel occupying the planes $z=\pm d/2$ are of infinite extent, all the physical quantities depend upon only on *z* and *t* only. Under the Boussinesq approximation, the flow through porous medium is governed by the equations with reference to a rotating frame are

$$\frac{\partial w}{\partial z}=0 \tag{2.1}$$

$$\frac{\partial u}{\partial t}-2i\Omega v+w_0\frac{\partial u}{\partial z}=-\frac{1}{\rho}\frac{\partial p}{\partial x}+\nu\frac{\partial^2 u}{\partial z^2}+\frac{\alpha_1}{\rho}\frac{\partial^3 u}{\partial z^2\partial t}-\frac{\sigma B_0^2}{\rho}u-\frac{\nu}{k}u+g\beta T+g\beta_c C \tag{2.2}$$

$$\frac{\partial v}{\partial t}+2i\Omega u+w_0\frac{\partial v}{\partial z}=-\frac{1}{\rho}\frac{\partial p}{\partial y}+\nu\frac{\partial^2 v}{\partial z^2}+\frac{\alpha_1}{\rho}\frac{\partial^3 z}{\partial z^2\partial t}-\frac{\sigma B_0^2}{\rho}u-\frac{\nu}{\kappa}v \tag{2.3}$$

$$\rho C_p\left(\frac{\partial T}{\partial t}+w_0\frac{\partial T}{\partial z}\right)=K_1\frac{\partial^2 T}{\partial z^2}-Q_0T+Q_1C-\frac{\partial q_1}{\partial z} \tag{2.4}$$

$$\frac{\partial C}{\partial t}+w_0\frac{\partial C}{\partial z}=D\frac{\partial^2 T}{\partial z^2}-K_cC \tag{2.5}$$

The boundary conditions are

$$u=\frac{2-f_1L}{f_1}\frac{\partial u}{\partial z}=L\frac{\partial u}{\partial z},\ v=\frac{2-f_1L}{f_1}\frac{\partial v}{\partial z}=L\frac{\partial v}{\partial z},\ T=0, C=0, \text{ at } z=-\frac{d}{2} \tag{2.6}$$

©2006-2019 Asian Research Publishing Network (ARPN). All rights reserved.

$$u = v = 0,\ T = T_0 \cos \omega t, C = C_0 \cos \omega t \text{ at } z = \frac{d}{2} \quad (2.7)$$

Where, $L = \mu \left(\frac{\pi}{2p\rho} \right)^{1/2}$ is the mean free path which is constant for an incompressible fluid.

Following Cogley *et al* [16] the last term in the energy equation stand for radiative heat flux which is given by

$$\frac{\partial q_1}{\partial z} = 4\alpha^2 T \quad (2.8)$$

Where α is the mean variation absorption coefficient?

Introducing non-dimensional variables,

$$z^* = \frac{z}{d}, x^* = \frac{x}{d}, y^* = \frac{y}{d}, u^* = \frac{u}{d}, v^* = \frac{v}{d}, \theta = \frac{T}{T_0}, \phi = \frac{C}{C_0}, t^* = \frac{t w_0}{d}, p^* = \frac{p}{\rho w_0^2}, \omega^* = \frac{\omega d}{w_0}$$

Making use of non-dimensional variables, the equations (2.2), (2.3), (2.4) and (2.5) reduces to (dropped asterisks)

$$\mathrm{Re}\left(\frac{\partial u}{\partial t} + \frac{\partial u}{\partial z} \right) - 2iRv = -\mathrm{Re}\frac{\partial p}{\partial x} + \frac{\partial^2 u}{\partial z^2} + S\frac{\partial^3 u}{\partial z^2 \partial t} - \left(M^2 + \frac{1}{K} \right) u + \mathrm{Gr}\,\theta + \mathrm{Gc}\,\phi \quad (2.9)$$

$$\mathrm{Re}\left(\frac{\partial v}{\partial t} + \frac{\partial v}{\partial z} \right) + 2iRu = -\mathrm{Re}\frac{\partial p}{\partial y} + \frac{\partial^2 v}{\partial z^2} + S\frac{\partial^3 v}{\partial z^2 \partial t} - -\left(M^2 + \frac{1}{K} \right) v \quad (2.10)$$

$$\mathrm{Re}\,\mathrm{Pr}\left(\frac{\partial \theta}{\partial t} + \frac{\partial \theta}{\partial z} \right) = \frac{\partial^2 \theta}{\partial z^2} - \mathrm{Pr}\,\phi_1 \theta + \mathrm{Re}^2\,\mathrm{Pr}\,Q\phi - \mathrm{Pr}\,N^2\theta \quad (2.11)$$

$$\mathrm{Sc}\,\mathrm{Re}\left(\frac{\partial \phi}{\partial t} + \frac{\partial \phi}{\partial z} \right) = \frac{\partial^2 \phi}{\partial z^2} - \mathrm{Sc}\,\mathrm{Re}\,\mathrm{Kc}\,\phi \quad (2.12)$$

The corresponding boundary conditions in non dimensional form are

$$u = h\frac{\partial u}{\partial z},\ v = h\frac{\partial v}{\partial z},\ T = 0, C = 0 \text{ at } z = -\frac{1}{2} \quad (2.13)$$

$$u = v = 0,\ T = T_0 \cos \omega t, C = C_0 \cos \omega t \text{ at } z = \frac{1}{2} \quad (2.14)$$

Where, $\mathrm{Re} = \frac{w_0 d}{\nu}$ is Reynolds number, $R = \frac{\Omega d^2}{\nu}$ is the rotation parameter, $K = \frac{k}{d^2}$ is the permeability parameter, $\mathrm{Gr} = \frac{g\beta d^2 T_0}{\nu w_0}$ is the thermal Grashof number, $\mathrm{Gc} = \frac{g\beta_c d^2 C_0}{\nu w_0}$ is the mass Grashof number, $\mathrm{Pr} = \frac{\mu C_p}{K_1}$ is the Prandtl number, $\mathrm{Sc} = \frac{\nu}{D}$ is the Schmidt number, $\mathrm{Kc} = \frac{K_c d}{w_0}$ is the chemical reaction parameter, $N = \frac{2\alpha d}{\sqrt{K_1}}$ is the Radiation parameter, $\phi_1 = \frac{Q_0 d^2}{\mu C_p}$ is the Heat absorption parameter, $Q = \frac{Q_1 \nu C_0}{\rho C_p w_0^2 T_0}$ is the Radiation absorption number, $M^2 = \frac{\sigma B_0^2 d^2}{\mu}$ is the Hartmann number and $S = \frac{\alpha_1}{\rho d^2}$ is the second grade fluid parameter.

Combining equations (2.9) and (2.10), let $q = u + iv$ and $\xi = x - iy$, we obtain

$$\mathrm{Re}\left(\frac{\partial q}{\partial t} + \frac{\partial q}{\partial z} \right) = -\mathrm{Re}\frac{\partial p}{\partial \xi} + \frac{\partial^2 q}{\partial z^2} + S\frac{\partial^3 q}{\partial z^2 \partial t} - \left(M^2 + 2iR + \frac{1}{K} \right) q + \mathrm{Gr}\,\theta + \mathrm{Gc}\,\phi \quad (2.15)$$

We assume the flow under the influence of pressure gradient varying periodically with time,

©2006-2019 Asian Research Publishing Network (ARPN). All rights reserved.

$$-\frac{\partial p}{\partial \xi} = A\cos\omega t \tag{2.16}$$

$$\mathrm{Re}\left(\frac{\partial q}{\partial t}+\frac{\partial q}{\partial z}\right) = \mathrm{Re}\,A\cos\omega t + \frac{\partial^2 q}{\partial z^2} + S\frac{\partial^3 q}{\partial z^2 \partial t} - \left(M^2 + 2iR + \frac{1}{K}\right)q + \mathrm{Gr}\,\theta + \mathrm{Gc}\,\phi \tag{2.17}$$

The corresponding boundary conditions are

$$q = h\frac{\partial q}{\partial z},\ \theta = 0,\ \phi = 0 \qquad \text{at} \quad z = -\frac{1}{2} \tag{2.18}$$

$$q = 0, \theta = \cos\omega t,\ \phi = \cos\omega t \qquad \text{at} \quad z = \frac{1}{2} \tag{2.19}$$

In order to solve the equations (2.17), (2.11) and (2.12) with the boundary conditions (2.18) & (2.19) following Choudary *et al.* [17] we assume the solution of the form

The equation (2.16) is substituting in the equation (2.15) we obtain

$$q(z,t) = q_0(z)e^{i\omega t} \tag{2.20}$$

$$\theta(z,t) = \theta_0(z)e^{i\omega t} \tag{2.21}$$

$$\phi(z,t) = \phi_0(z)e^{i\omega t} \tag{2.22}$$

Substituting the equations (2.20), (2.21) and (2.22) in (2.17), (2.11) and (2.12) respectively, the resulting equations are,

$$(1+Si\omega)\frac{d^2 q_0}{dz^2} - \mathrm{Re}\frac{dq_0}{dz} - \left(\frac{M^2}{1-im} + \frac{1}{K} + i(2R+\omega\,\mathrm{Re})\right)q_0 = -\mathrm{Re}\,A - \mathrm{Gr}\,\theta_0 - \mathrm{Gr}\,\phi_0 \tag{2.23}$$

$$\frac{d^2\theta_0}{dz^2} - \mathrm{Re\,Pr}\frac{d\theta_0}{dz} - \left(\mathrm{Pr}\,\phi + \mathrm{Pr}\,N^2 + i\omega\,\mathrm{Re\,Pr}\right)\theta_0 + \mathrm{Re}^2\,\mathrm{Pr}\,Q\phi_0 = 0 \tag{2.24}$$

$$\frac{d^2\phi_0}{dz^2} - \mathrm{ReSc}\frac{d\phi_0}{dz} - (i\omega + \mathrm{Kc})\,\mathrm{ReSc}\,\phi_0 = 0 \tag{2.25}$$

The corresponding boundary conditions are

$$q_0 = h\frac{\partial q}{\partial z},\ \ \theta_0 = 0,\ \phi_0 = 0 \qquad \text{at} \quad z = -\frac{1}{2} \tag{2.26}$$

$$q_0 = 0,\ \ \theta_0 = 1,\ \phi_0 = 1 \qquad \text{at} \quad z = \frac{1}{2} \tag{2.27}$$

Solving the equations (2.23), (2.24) and (2.25) with respect to the boundary conditions (2.26) and (2.27), we obtained the following expressions for the velocity and temperature.

$$q(z,t) = \Big\{B_3\cosh m_1 z + B_4\sinh m_2 z + \frac{\mathrm{Re}\,A}{a_1} - \frac{\mathrm{Gr}B_1}{2}\left(\frac{e^{m_3 z}}{a_2} + \frac{e^{-m_3 z}}{a_3}\right) - \frac{\mathrm{Gr}B_2}{2}8\left(\frac{e^{m_4 z}}{a_4} + \frac{e^{-m_4 z}}{a_5}\right) - A_8 e^{\left(\frac{1}{2}+z\right)m_5} + A_9 e^{\left(\frac{1}{2}+z\right)m_6}\Big\}e^{i\omega t} \tag{2.28}$$

$$\theta = \left\{B_1\cosh m_3 z + B_2\sinh m_4 z + \frac{\mathrm{Pr\,Re}^2\,Q}{e^{m_5}-e^{m_6}}\left(\frac{e^{\left(\frac{1}{2}+z\right)m_5}}{m_5^2 - \mathrm{RePr}\,m_5 - b_1^2} - \frac{e^{\left(\frac{1}{2}+z\right)m_6}}{m_6^2 - \mathrm{RePr}\,m_6 - b_1^2}\right)\right\}e^{i\omega t} \tag{2.29}$$

$$\phi = \frac{1}{e^{m_5}-e^{m_6}}\left\{e^{\left(\frac{1}{2}+z\right)m_5} - e^{\left(\frac{1}{2}+z\right)m_6}\right\}e^{i\omega t} \tag{2.30}$$

All the constants used above have been mentioned in the appendix.

The validity and the correctness of the present solution are verified by taking $S = \mathrm{Gr} = M = R = h = 0$ and $K \to \infty$.

i.e., for the horizontal channel in the absence of rotation, slip flow and the condition of the ordinary medium so that

$$q(z,t) = \frac{A}{i\omega}\left\{1 - \frac{\cosh\left(\frac{\mathrm{Re}+\sqrt{\mathrm{Re}^2+4i\omega\,\mathrm{Re}}}{2}\right)z}{\cosh\left(\frac{\mathrm{Re}+\sqrt{\mathrm{Re}^2+4i\omega\,\mathrm{Re}}}{2}\right)}\right\}e^{i\omega t} \tag{2.31}$$

©2006-2019 Asian Research Publishing Network (ARPN). All rights reserved.

This solution reported by Schlichting and Gersten [18] for periodic variation of the pressure gradient along axis of the channel.

We find the Skin Fraction τ_L at the left plate in terms of its amplitude and the phase angle as

$$\tau_L = \left(\frac{\partial q}{\partial z}\right)_{z=-\frac{1}{2}} = |q|\cos(\omega t + \gamma)$$

$$q_r + iq_i = B_3 m_1 \sinh\left(\frac{m_1}{2}\right) + B_4 m_2 \cosh\left(\frac{m_2}{2}\right) - \frac{\mathrm{Gr}B_1 m_3}{2}\left(\frac{e^{-\frac{m_3}{2}}}{a_2} - \frac{e^{\frac{m_3}{2}}}{a_3}\right) - \frac{\mathrm{Gr}B_2 m_4}{2}\left(\frac{e^{-\frac{m_4}{2}}}{a_4} - \frac{e^{\frac{m_4}{2}}}{a_5}\right) - A_8 m_5 + A_9 m_6 \quad (2.32)$$

The amplitude is given by

$$q = \sqrt{q_r^2 + q_i^2}$$

And phase angle is given by

$$\gamma = \tan^{-1}\left(\frac{q_i}{q_r}\right)$$

The rate of heat transfer (N_U) in terms of amplitude and the phase angle can be obtained as

$$Nu = \left(\frac{\partial T}{\partial z}\right)_{z=-\frac{1}{2}} = |r|\cos(\omega t + \psi)$$

$$r_r + ir_i = -B_1 m_3 \sinh\left(\frac{m_3}{2}\right) + B_2 m_4 \cosh\left(\frac{m_4}{2}\right) + \frac{\mathrm{Pr}\,\mathrm{Re}^2 Q}{e^{m_5} - e^{m_6}}\left(\frac{m_5}{m_5^2 - \mathrm{Re}\,\mathrm{Pr}\,m_5 - b_1^2} - \frac{m_6}{m_6^2 - \mathrm{Re}\,\mathrm{Pr}\,m_6 - b_1^2}\right)e^{i\omega t} \quad (2.33)$$

Where,

The amplitude $r = \sqrt{r_r^2 + r_i^2}$

And phase angle $\psi = \tan^{-1}\left(\frac{r_i}{r_r}\right)$

The rate of mass transfer (Sh) in terms of amplitude and the phase angle can be obtained as

$$Sh = \left(\frac{\partial \phi}{\partial z}\right)_{z=-\frac{1}{2}} = |s|\cos(\omega t + \eta)$$

$$s_r + is_i = \frac{1}{e^{m_5} - e^{m_6}}\left(\frac{m_5}{2} - \frac{m_6}{2}\right) \quad (2.34)$$

Where,

The amplitude $|s| = \sqrt{s_r^2 + s_i^2}$

and phase angle $\eta = \tan^{-1}\left(\frac{s_i}{s_r}\right)$

3. RESULTS AND DISCUSSIONS

The velocity profiles depict from the Figures (2-15) while the temperature and concentration profiles from the Figures (16-19) and Figures (20-21) respectively. Also the skin friction, Nusselt number and Sherwood number calculated and are tabulated in the Tables (1-3). The effect of the Rotation number *R* on the velocity profile shown by the Figure-2. We noticed that the magnitude of velocity components *u* and *v* enhance with increasing *R* throughout the fluid region. Similarly the resultant velocity is also enhances with increasing rotation parameter *R*. From Figure-3 we observed that, the magnitude of the velocity components *u* and *v* reduces with increasing Hartmann number M. Further, due to interaction of applied magnetic field with conducting fluid the current is generated. Consequently, it gives rise to an induced magnetic field and ponders motive force. That force acts opposite to the direction of the flow and unless an additional electric field is applied to counter act. In the present study the Lorentz force decelerates the fluid flow consequently resulted in thinning of boundary layer. The resultant velocity is also reduces with increasing in M. The velocity component *u* and *v* enhance throughout the fluid region with increasing permeability parameter K. Hence, the resultant velocity enhances with increasing the permeability parameter *K* throughout the fluid region. We also observe that lower the permeability lesser the fluid speed in the entire fluid medium (Figure-4). Similar behaviour is observed for increasing second grade fluid parameter S, thermal Grashof number Gr, and mass Grashof number Gc (Figures 5-7). It is observed from the Figures (8-11) that the velocity profiles are diminished with the increase of all these parameters Prandtl number Pr, radiation parameter *N*, slip parameter *h* and the radiation absorption parameter *Q*. The resultant velocity is also reduces with increasing Pr or *h* or Q or N. Presence of source reduces the velocity, significantly in all the layers. Most interesting case is due to the presence of sink which gives rise to a span wise oscillatory flow after a few layers from the plate. This is due to depletion of thermal energy causing a sudden reduction of velocity. The magnitudes of the velocity components *u* and *v* boost up with increasing in the amplitude of the pressure gradient *A* (Figure-12). It is observed from these Figures (13-15) that the velocity profile is diminished with the increase of all these parameters heat absorption parameter ϕ_1, the frequency of oscillation ω and chemical reaction parameter Kc. That is it starts decreasing near the left plate of the channel. The resultant velocity is also shown the same behaviour as that of *u* and *v* for all the variations in the governing parameters.

The variations in the temperature profile are presented in the Figures (16-19). It is observed from this Figure-16 that the temperature profiles decrease with the increasing Reynolds number Re and the Prandtl number

©2006-2019 Asian Research Publishing Network (ARPN). All rights reserved.

Pr. The similar behaviour is observed with increasing the radiation parameter *N* and Schmidt number Sc. The temperature profile is diminished with increasing chemical reaction parameter Kc, the radiation absorption parameter *Q*, the frequency of oscillation ω and it increases with the heat absorption parameter for $0 \le \phi_1 \le 1$ and decreases for $\phi_1 \ge 1$ (Figures. 17-19).

A variation in the concentration profile is plotted in the Figures (20-21) and it is evident from the study of this figure that the amplitude of the concentration profile decreases with all the parameters Reynolds number Re, chemical reaction parameter Kc, Schmidt number Sc and the frequency of oscillation ω effecting the concentration equation.

The skin friction, Nusselt number and Sherwood number are evaluated analytically and tabulated in the tables. The amplitude and phase angle of the skin friction are shown in Table-1. The negative values in this table indicate that there is always a phase lag and this phase goes on increasing with increasing frequency of oscillation. We noticed that, the amplitude of stress $|q|$ and phase angle γ are enhanced with increasing the parameters *K*, *R*, *S*, Gr and Kc. Likewise the amplitude of the stress and the magnitude of the phase angle increases with Gc, Pr, *N*, *A*, *Q* and ϕ_1. The amplitude of stress $|q|$ reduces and phase angle γ increases with increasing *M*, *h* and ω. The reversal behaviour is observed with increasing *m* and Sc. From the Table-2, we found that the amplitude $|r|$ and phase angle ψ of the Nusselt number increases with increasing Re, Pr, Sc and Kc. Also the amplitude of the Nusselt number decreases while phase angle ψ of the Nusselt number increases with increasing with N, ϕ_1 and ω. The opposite behaviour is observed with increasing *Q*. Finally, From the Table-3, we found that the amplitude $|s|$ and phase angle η of the Sherwood number decreases with increasing Re, Kc and ω. Also the amplitude of the Sherwood number decreases while phase angle ψ of the Sherwood number increases with increasing with Sc.

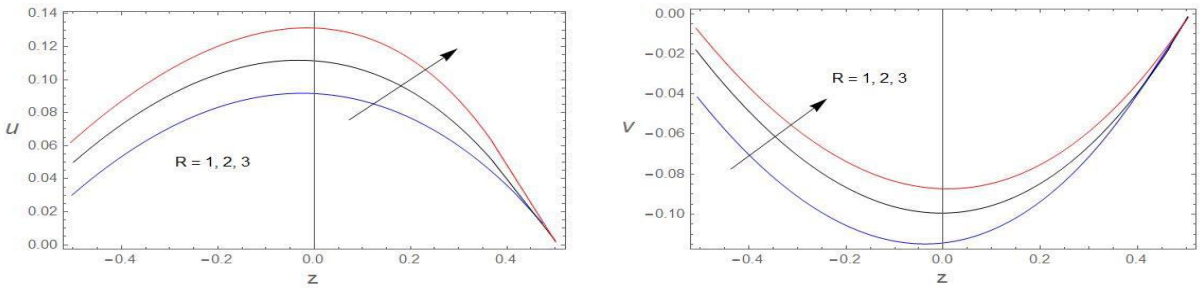

Figure-2. The velocity profiles for u and v against R with
$\mathrm{Gr} = 3, S = 1, M = 1, \mathrm{Pr} = 0.71, K = 1, A = 5, h = 0.2, \phi_1 = 0.1, N = 1, \omega = \pi/6, \mathrm{Gc} = 5, \mathrm{Kc} = 1, Q = 1$.

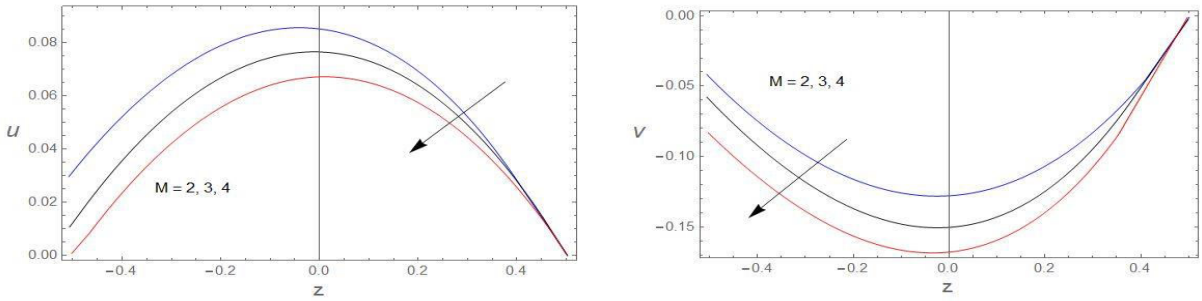

Figure-3. The velocity profiles for u and v against M with
$\mathrm{Gr} = 3, S = 1, R = 1, \mathrm{Pr} = 0.71, K = 1, A = 5, h = 0.2, \phi_1 = 0.1, N = 1, \omega = \pi/6, \mathrm{Gc} = 5, \mathrm{Kc} = 1, Q = 1$.

©2006-2019 Asian Research Publishing Network (ARPN). All rights reserved.

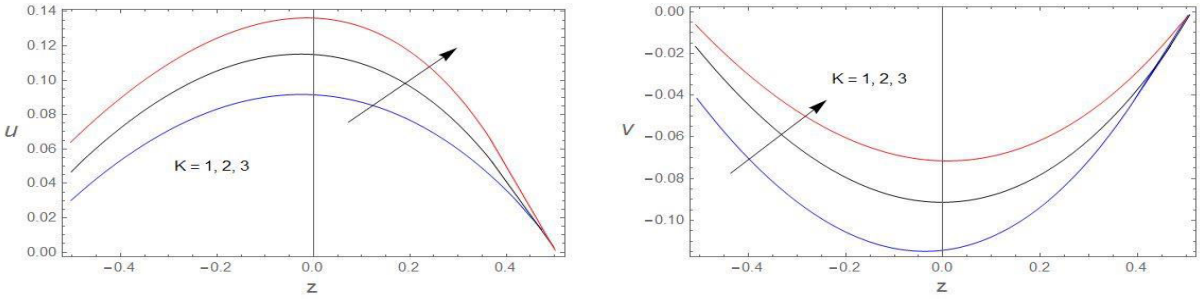

Figure-4. The velocity profiles for u and v against K with
$\mathrm{Gr}=3, S=1, M=1, \mathrm{Pr}=0.71, \mathrm{R}=1, A=5, h=0.2, \phi_1=0.1, N=1, \omega=\pi/6, \mathrm{Gc}=5, \mathrm{Kc}=1, Q=1$.

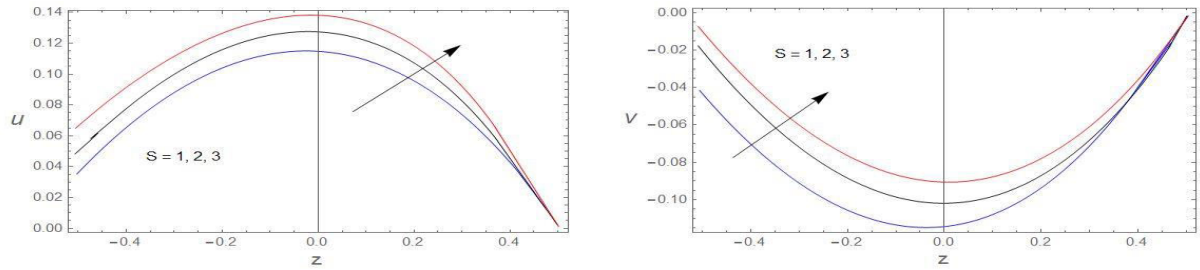

Figure-5. The velocity profiles for u and v against S with
$\mathrm{Gr}=3, R=1, M=1, \mathrm{Pr}=0.71, K=1, A=5, h=0.2, \phi_1=0.1, N=1, \omega=\pi/6, \mathrm{Gc}=5, \mathrm{Kc}=1, Q=1$.

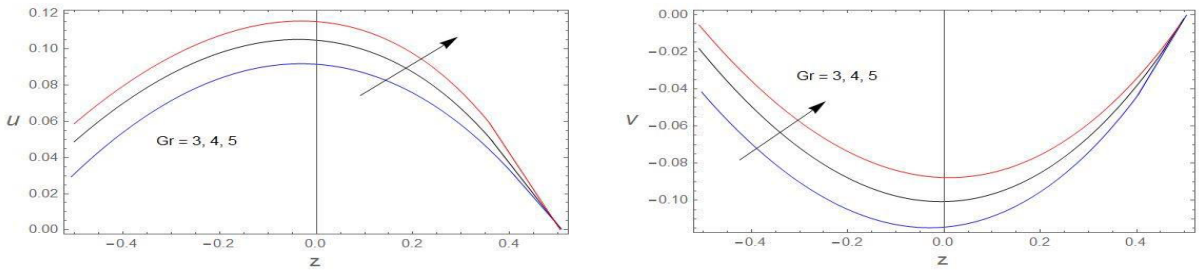

Figure-6. The velocity profiles for u and v against Gr with
$\mathrm{R}=1, S=1, M=1, \mathrm{Pr}=0.71, K=1, A=5, h=0.2, \phi_1=0.1, N=1, \omega=\pi/6, \mathrm{Gc}=5, \mathrm{Kc}=1, Q=1$.

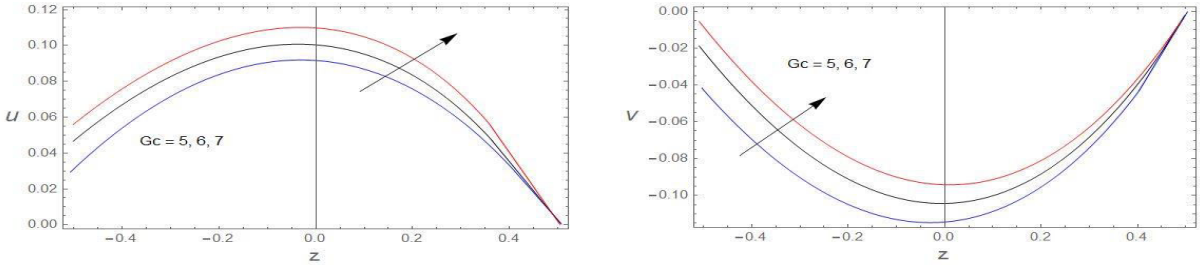

Figure-7. The velocity profiles for u and v against Gc with
$\mathrm{Gr}=3, S=1, M=1, \mathrm{Pr}=0.71, K=1, A=5, h=0.2, \phi_1=0.1, N=1, \omega=\pi/6, R=1, \mathrm{Kc}=1, Q=1$.

©2006-2019 Asian Research Publishing Network (ARPN). All rights reserved.

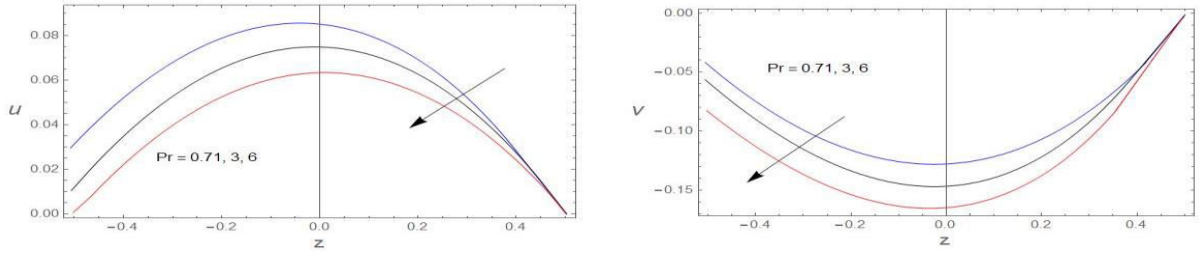

Figure-8. The velocity profiles for u and v against Pr with
$\mathrm{Gr}=3, S=1, M=1, \mathrm{R}=1, K=1, A=5, h=0.2, \phi_1=0.1, N=1, \omega=\pi/6, \mathrm{Gc}=5, \mathrm{Kc}=1, Q=1$.

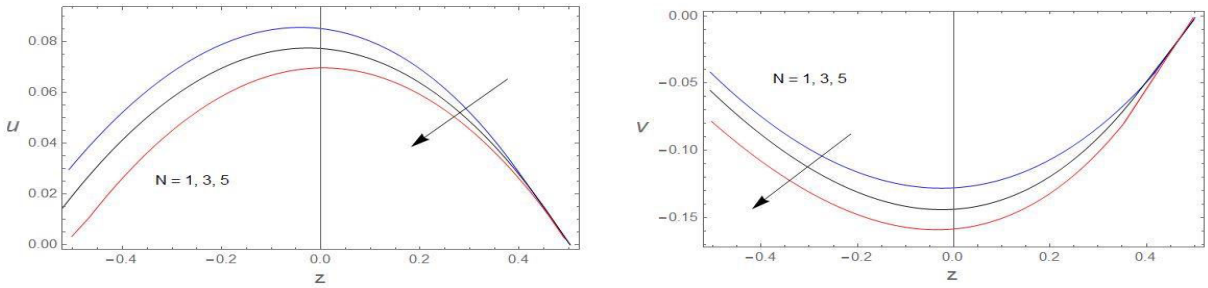

Figure-9. The velocity profiles for u and v against N with
$\mathrm{Gr}=3, S=1, M=1, \mathrm{Pr}=0.71, K=1, A=5, h=0.2, \phi_1=0.1, R=1, \omega=\pi/6, \mathrm{Gc}=5, \mathrm{Kc}=1, Q=1$.

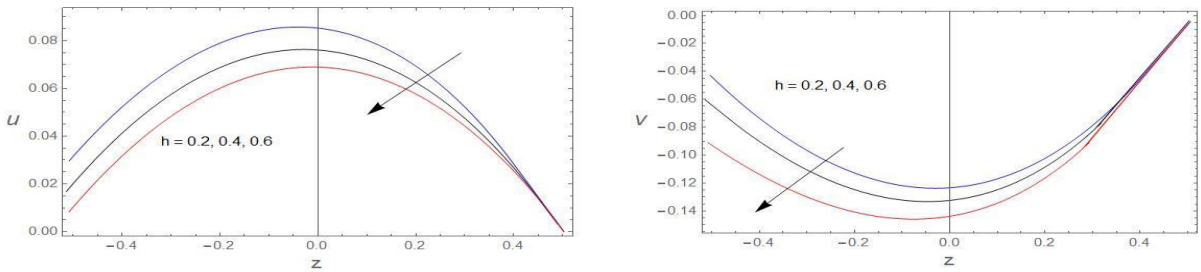

Figure-10. The velocity profiles for u and v against h with
$\mathrm{Gr}=3, S=1, M=1, \mathrm{Pr}=0.71, K=1, A=5, \mathrm{R}=1, \phi_1=0.1, N=1, \omega=\pi/6, \mathrm{Gc}=5, \mathrm{Kc}=1, Q=1$.

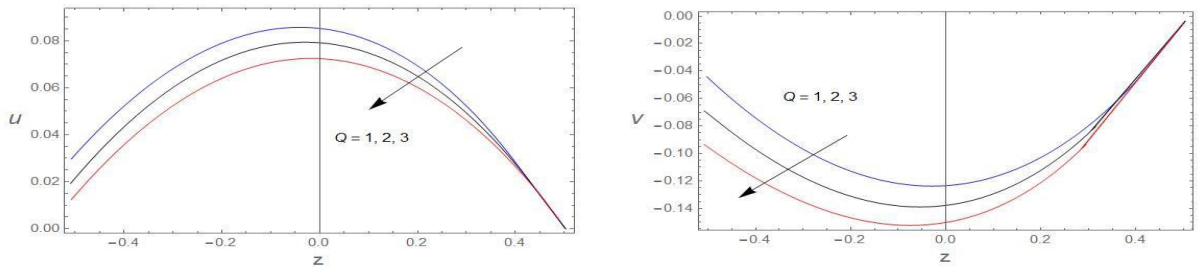

Figure-11. The velocity profiles for u and v against Q with
$\mathrm{Gr}=3, S=1, M=1, \mathrm{Pr}=0.71, K=1, A=5, h=0.2, \phi_1=0.1, N=1, \omega=\pi/6, \mathrm{Gc}=5, \mathrm{Kc}=1, R=1$.

©2006-2019 Asian Research Publishing Network (ARPN). All rights reserved.

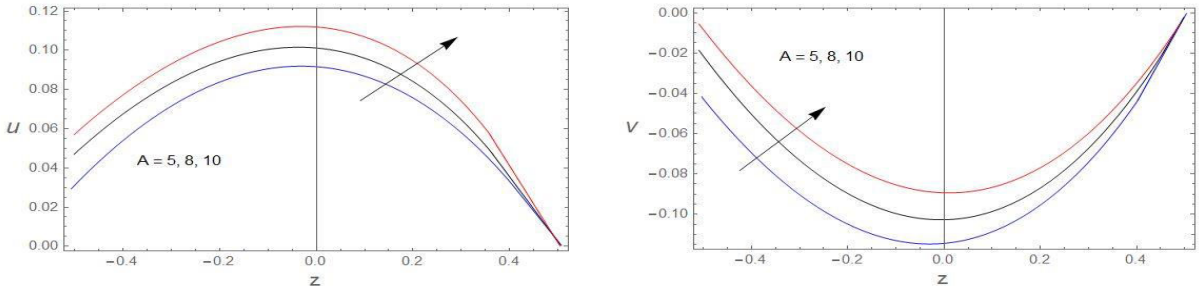

Figure-12. The velocity profiles for u and v against A with
$\mathrm{Gr}=3, S=1, M=1, \mathrm{Pr}=0.71, K=1, \mathrm{R}=1, h=0.2, \phi_1=0.1, N=1, \omega=\pi/6, \mathrm{Gc}=5, \mathrm{Kc}=1, Q=1$.

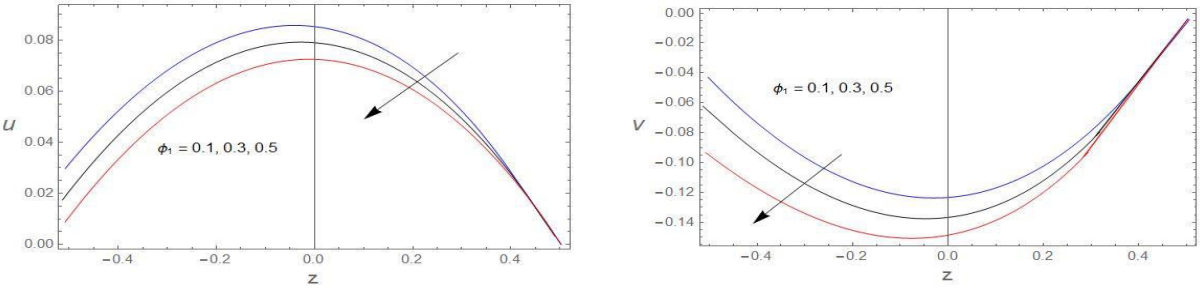

Figure-13. The velocity profiles for u and v against ϕ_1 with
$\mathrm{Gr}=3, S=1, M=1, \mathrm{Pr}=0.71, K=1, A=5, h=0.2, R=1, N=1, \omega=\pi/6, \mathrm{Gc}=5, \mathrm{Kc}=1, Q=1$.

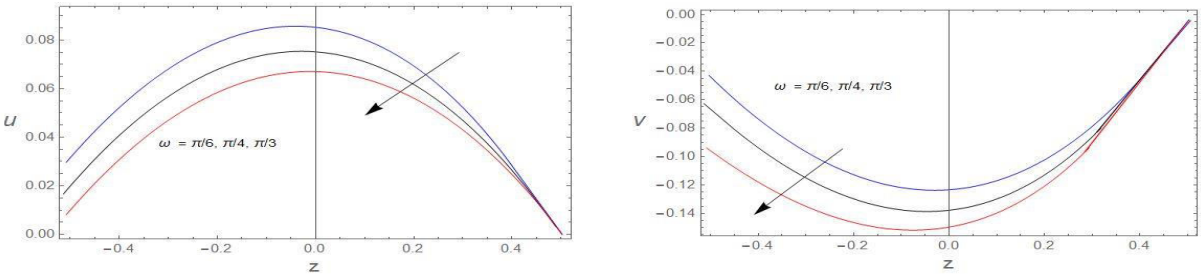

Figure-14. The velocity profiles for u and v against ω with
$\mathrm{Gr}=3, S=1, M=1, \mathrm{Pr}=0.71, K=1, A=5, h=0.2, \phi_1=0.1, N=1, R=1, \mathrm{Gc}=5, \mathrm{Kc}=1, Q=1$.

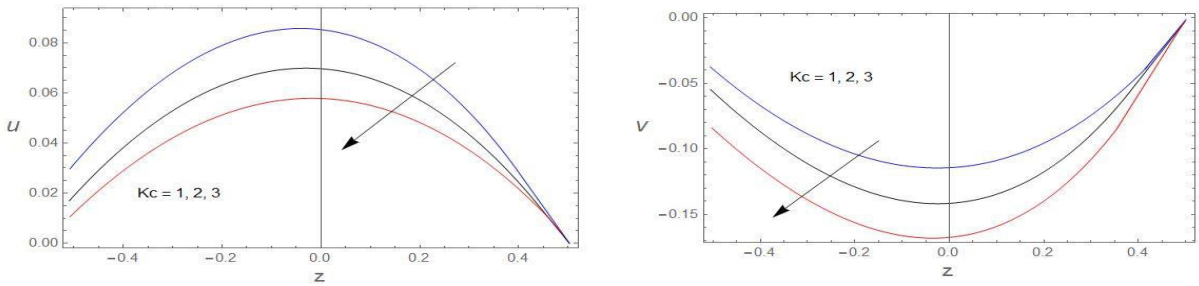

Figure-15. The velocity profiles for u and v against Kc with
$\mathrm{Gr}=3, S=1, M=1, \mathrm{Pr}=0.71, K=1, A=5, h=0.2, \phi_1=0.1, N=1, \omega=\pi/6, \mathrm{Gc}=5, R=1, Q=1$.

©2006-2019 Asian Research Publishing Network (ARPN). All rights reserved.

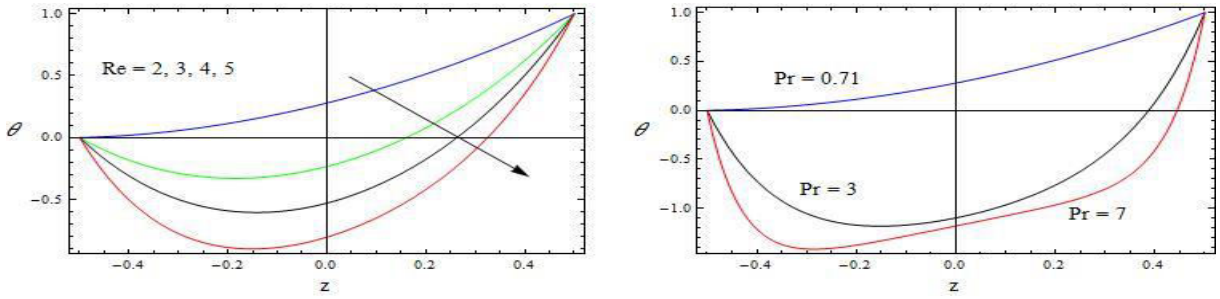

Figure-16. The Temperature profiles for θ against Re and Pr $Q = 0.5, \mathrm{Sc} = 0.22, \mathrm{Kc} = 1, \phi_1 = 0.1, \omega = \pi/6, N = 1$.

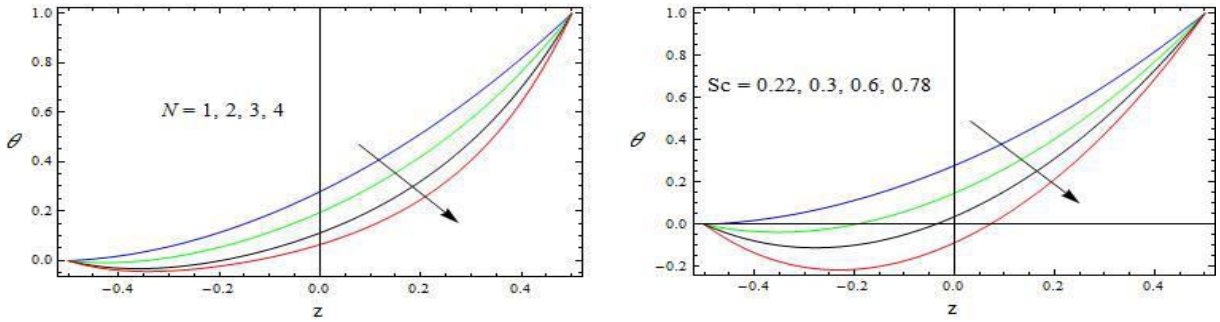

Figure-17. The Temperature profiles for θ against Re and Pr $\mathrm{Re} = 2, Q = 0.5, \mathrm{Kc} = 1, \phi_1 = 0.1, \omega = \pi/6, \mathrm{Pr} = 0.71$.

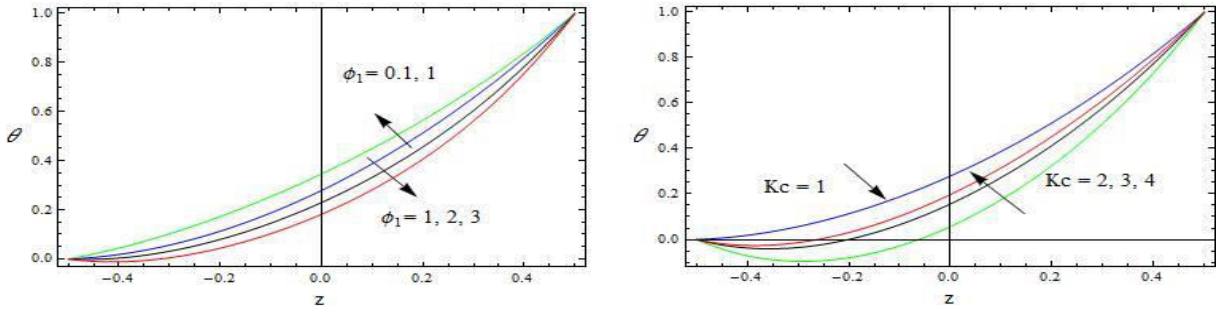

Figure-18. The Temperature profiles for θ against ϕ_1 and Kc $\mathrm{Re} = 2, Q = 0.5, \mathrm{Sc} = 0.22, \omega = \pi/6, \mathrm{Pr} = 0.71, N = 1$.

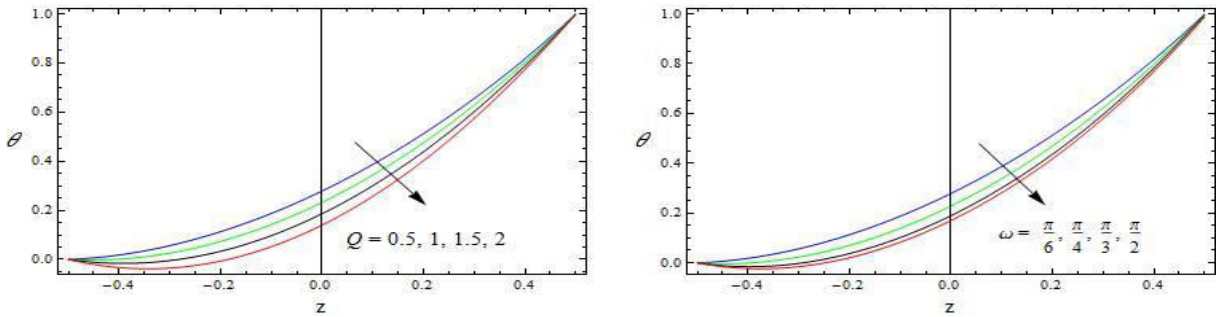

Figure-19. The Temperature profiles for θ against Q and ω $\mathrm{Re} = 2, \mathrm{Sc} = 0.22, \mathrm{Kc} = 1, \phi_1 = 0.1, \mathrm{Pr} = 0.71, N = 1$.

©2006-2019 Asian Research Publishing Network (ARPN). All rights reserved.

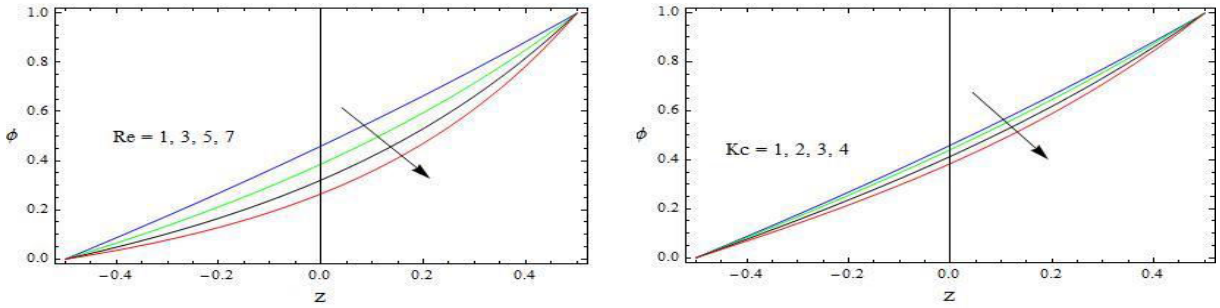

Figure-20. The Concentration profiles for ϕ against Re and Kc with $\mathrm{Sc} = 0.22, \omega = \pi / 6$.

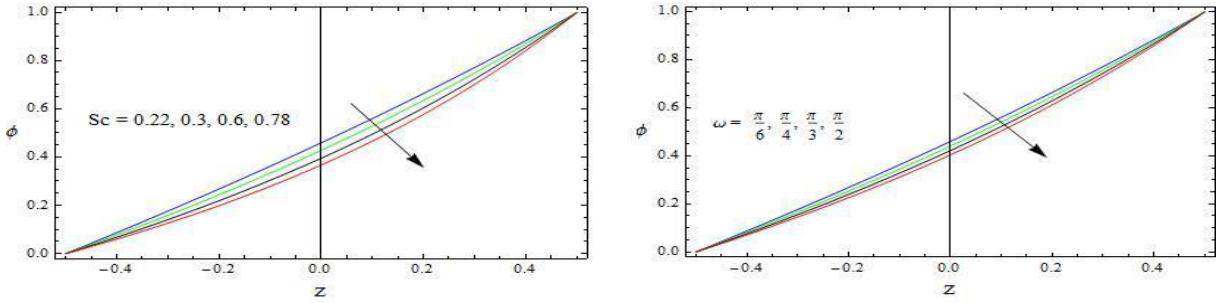

Figure-21. The Concentration profiles for ϕ against Sc and ω with $\mathrm{Sc} = 0.22, \omega = \pi / 6$.

©2006-2019 Asian Research Publishing Network (ARPN). All rights reserved.

Table-1. Amplitude and Phase angle of Skin friction for $\mathrm{Re} = 0.5,\ t = 0.1$.

M	K	R	S	Gr	Gc	Pr	N	A	h	ω	Q	Kc	Sc	ϕ_1	Amplitude $\lvert q \rvert$	Phase angle γ
0.5	**0.5**	**1**	**1**	**3**	**5**	**0.71**	**1**	**5**	**0.2**	$\pi/6$	**1**	**1**	**0.22**	**1**	**2.39965**	**0.281014**
1															2.07458	0.488599
1.5															1.82114	0.911415
	1														4.10478	0.360225
	2														4.73362	0.532566
		1.5													2.59885	0.699859
		2													2.92554	0.947748
			2												3.54774	0.433652
			3												4.52214	0.525514
				4											6.09661	1.201125
				5											10.7485	1.385595
					6										2.74745	-0.490145
					7										4.17254	-0.91221
						3									3.39665	-1.20552
						7									4.97784	-2.16045
							2								3.95895	-0.85012
							3								5.34219	-0.97254
								7							3.50025	-0.33025
								9							5.24474	-0.59662
									0.3						2.35520	0.39665
									0.4						2.32356	0.48875
										$\pi/4$					1.70122	1.33625
										$\pi/3$					0.16585	1.50014
											2				17.5011	-1.51445
											3				34.5415	-2.44478
												2			3.39332	0.43256
												3			4.82145	0.59985
													0.3		5.69969	0.15526
													0.6		28.5011	0.08854
														1.5	7.43325	-0.69958
														2	9.72114	-0.88859

©2006-2019 Asian Research Publishing Network (ARPN). All rights reserved.

Table-2. Amplitude and Phase angle of Nusselt number for $t = 0.1$.

Re	Pr	N	ϕ_1	Sc	Kc	Q	ω	Amplitude $\lvert r \rvert$	Phase angle ψ
2	0.71	1	0.2	0.22	0.2	1	$\pi/6$	4.31112	0.538747
3								12.6750	1.230090
4								16.1478	1.527450
	3							21.6871	1.405730
	7							45.0290	1.536470
		2						4.22257	1.466980
		3						3.93830	1.491090
			0.5					2.79348	0.667940
			1					2.33856	1.104290
				0.3				5.57300	0.627978
				0.6				16.0440	1.447030
					0.4			5.36079	1.377640
					0.6			5.82016	1.541990
						2		7.58466	0.355346
						3		10.9587	0.283540
							$\pi/4$	4.27767	0.853784
							$\pi/3$	4.15536	1.011080

Table-3. Amplitude and Phase angle of Sherwood number for $t = 0.1$.

Re	Sc	Kc	ω	Amplitude $\lvert s \rvert$	Phase angle η
2	**0.22**	**0.2**	$\pi/6$	**0.740534**	**1.55564**
3				0.634072	-1.55232
4				0.541233	-1.55138
	0.3			0.661697	1.56853
	0.6			0.427695	1.62798
		0.4		0.690418	1.55465
		0.6		0.644864	1.55373
			$\pi/4$	0.740284	1.54805
			$\pi/3$	0.739937	1.54045

4. CONCLUSIONS

a) The resultant velocity enhance with increasing *R*, *S* and *K* throughout the fluid region.

b) The velocity profile is diminished with the increasing ω, *M* and *N*.

c) The temperature profiles decrease with the increasing Pr and *N*.

d) The concentration profile decreases with all Kc and ω.

e) The amplitude of stress reduces and phase angle increases with increasing *M*, *h* and ω. The reversal behaviour is observed with increasing *m* and Sc.

f) The amplitude of the Sherwood number decreases while phase angle of the Sherwood number increases with increasing with Sc.

REFERENCES

[1] Marques WJr, Kremer M. and Shapiro F.M. 2000. Couette Flow with Slip and Jump Boundary

©2006-2019 Asian Research Publishing Network (ARPN). All rights reserved.

Conditions, Continuum Mech. Thermodynam. 12, pp. 379-386.

[2] Hayat T., Javed T. and Abbas Z. 2008. Slip flow and heat transfer of a second grade fluid past a stretching sheet through a porous space, Int. J. Heat Mass transfer. 51, pp. 4528-4534.

[3] Maki E. R., Kuzma D., Donnelly, R. L. and Kim B. 1966. Magnetohydrodynamic lubrication flow between parallel plates, J. Fluid Mech. 26, pp. 537-543.

[4] Hughes W. F. and Elco R. A. 1962. Magneto hydrodynamic lubrication flow between parallel rotating discs, J. Fluid Mech. 13, pp. 21-32.

[5] Hamza E. A. 1964. The magnetohydrodynamic squeeze film, J. Fluid Mech. 19, pp. 395-400.

[6] Hamza E. A. 1991. The magnetohydrodynamic effects on a fluid film squeezed between two rotating surfaces, J. Phys. D: Appl. Phys. 24, pp. 547-554.

[7] Bhattacharyya S. and Pal A. 1997. Unsteady MHD squeezing flow between two parallel rotating discs, Mech. Res. Commun. 24, pp. 615-623.

[8] Sweet Erik, Vajravelu K., Robert A. Gorder Van and Pop I. 2011. Analytical solution for the unsteady MHD flow of a viscous fluid between moving parallel plates, Commn. Nonlinear Sci. Numer. Simulat. 16, pp. 266-273.

[9] Hayat T., Fetecaua C. and Sajid M. 2008. Analytic solution for MHD transient rotating flow of a second grade fluid in a porous space. Nonlinear Analysis: Real World Applications. 9, pp. 1619-1627.

[10] Alagoa K. D., Tay G. and Abbey T.M. 1999. Radiative and free convective effects of a MHD flow through a porous medium between infinite parallel plates with time-dependent suction. Astrophysics and Space Science. 260, pp. 455-468.

[11] Mebine Promise and Gumus Rhoda H. 2010. On steady MHD thermally radiating and reacting thermosolutal viscous flow through a channel with porous medium, Int. J. of Mathematics and Mathematical sciences, Article ID287435, p. 12.

[12] VeeraKrishna. M and B.V. Swarnalathamma. 2016. Convective Heat and Mass Transfer on MHD Peristaltic Flow of Williamson Fluid with the Effect of Inclined Magnetic Field. AIP Conference Proceedings. 1728: 020461.

[13] Swarnalathamma. B. V. and M. Veera Krishna. 2016. Peristaltic hemodynamic flow of couple stress fluid through a porous medium under the influence of magnetic field with slip effect AIP Conference Proceedings. 1728: 020603.

[14] Veera Krishna. M and M. Gangadhar Reddy. 2016. MHD free convective rotating flow of Visco-elastic fluid past an infinite vertical oscillating porous plate with chemical reaction IOP Conf. Series: Materials Science and Engineering. 149: 012217.

[15] Veera Krishna. M and G. Subba Reddy. 2016. Unsteady MHD convective flow of Second grade fluid through a porous medium in a Rotating parallel plate channel with temperature dependent source IOP Conf. Series: Materials Science and Engineering. 149: 012216.

[16] Cogley A C, Vincenti W G, Gilles S E. 1968. American Institute of Aeronautics and Astronautics. 6, 551-553.

[17] Chaudhary R C, Jha, A K, Dhayal S S, J. 2006. Rajasthan Acad. Phy. Sci. 5(2): 233-238.

[18] Schlichting H, Gersten K. 2001. Boundary layer theory, 8th Edition, Springer-Verlag.